Effects of Relativistic and Absorption on ECE Spectra in High Temperature Tokamak Plasma

M. SATO and A. ISAYAMA

Japan Atomic Energy Agency, Naka Fusion Institute, Naka, Ibaraki 311-0193, Japan

(Received 5 January 2007 / Accepted 24 February 2007)

Using the extended Trubnikov's expression for the fully relativistic Maxwellian in the case of oblique propagation to the magnetic field (B_t), electron cyclotron emission (ECE) spectra are calculated in a high temperature (T_e) tokamak plasma. We investigate the ECE by changing the angles between the sight line and the equatorial plane or B_t direction. Feature of ECE spectra can be interpreted from the viewpoints of relativistic, Doppler and absorption effects. The downshift frequency variation due to the relativistic effect in the high field side (HFS) observation is bigger than that in the low field side observation. Absorption at the HFS plasma results in the deep dip at the HFS of fundamental, second and third harmonics in the ECE spectra. For the vertical observation, in the case of optically thin case, ECE spectra are similar to the emissivity profile, and when electron density (n_e) is higher, ECE spectra are modified due to the absorption in plasma. Since the B_t, n_e, T_e increase in the case of the SlimCS DEMO reactor, the ECE spectra expands to high frequency emission (~2000 GHz). So, ECE detector in the case of Fourier transform spectrometer system should be modified from present liquid He cooled InSb detector because of the detection of high frequency emission.

Keywords: electron cyclotron emission, oblique propagation, fully relativistic Maxwellian, absorption effect, tokamak

DOI: 10.1585/pfr.2.S1029

1. Introduction

Plasma confined in a magnetic field emits the electron cyclotron emission (ECE) [1,2]. The ECE in magnetic confinement devices has been used for the electron temperature (T_e) measurements [3]. For the measurement of electron temperature profile ($T_e(r)$) in tokamak, the second harmonic extraordinary mode of ECE in magnetic confined plasmas is usually observed in perpendicular to the magnetic field along the equatorial plane. When the T_e is low, the ECE spectrum from the low field side (LFS) observation is the same as that from high field side (HFS) observation. However, when the T_e is higher, the relativistic downshift frequency effect becomes very large, and the disagreement between spectra from LHS and HFS become large. By changing the angle (θ_{port}) between the sight line and the equatorial plane, the feature of ECE spectra is also changed due to the overlapping between harmonics, relativistic broadening and absorption effect in plasma. On the other hand, by changing the angle (θ_B) between sight line and the magnetic field (B_t), the Doppler broadening affects the ECE spectra.

Recently the analytic expression of emissivity for the oblique propagation to the magnetic field was obtained in the case of spherically symmetric Maxwellian distribution function [4, 5]. This expression is extended from the Trubnikov's equation [6] for the perpendicular propagation to that for the oblique propagation to the B_t. Using the extended Trubnikov's expression [5], the characteristic of ECE spectra on various sight line of observation are calculated in reactor grade tokamaks. The computational method is given in section 2. The calculation results are given in section 3. Summary is presented in section 4.

2. Computational Method

2.1 Extension of Trubnikov's equation

Emissivity for the perpendicular propagation to the B_t in the case of spherically symmetric relativistic Maxwellian velocity distribution function is given by Trubnikov [6]. Although the absorption coefficient for the oblique propagation to the B_t by weakly relativistic approximation is given by Fidone et al [8, 9] and Wu et al [10], there is no expression in the case of fully relativistic Maxwellian for the oblique propagation before recent EC14 conference [4,11]. So, for the oblique propagation to the B_t, an expression of emissivity was obtained in the case of the spherically symmetric relativistic Maxwellian velocity distribution function [4, 5]. This expression is extended from the Trubnikov's equation for the perpendicular propagation to that for the oblique propagation to the B_t. The extended Trubnikov's expression and the emissivities for various θ_B using the extended Trubnikov's expression are given in Ref. 5. The extended Trubnikov's expression can be obtained by the transformation from n, $\mathrm{d}\theta_\mathrm{p}$, and $\beta\cos\theta_\mathrm{p}$ in the Trubnikov's expression to $n/(1-\cos\theta_p\cos\theta_B)$, $\mathrm{d}\theta_p/(1-\cos\theta_p\cos\theta_B)$, $(\cos\theta_B-\beta\cos\theta_p)/\sin\theta_B$, appar-

author's e-mail: sato.masayasu@jaea.go.jp

ently. The n, and θ_p are the harmonic number, the angle between the velocity (v) and B_t in the momentum space, and $\beta = v/c$. The β is limited by the resonance condition. When the θ_B decreases, the peak of emissivity becomes small but the foot of the emissivity expands in the case of X mode. On the other hand in the case of O mode when the θ_B decreases, the peak of emissivity becomes big and the foot of the emissivity expands.

2.2 Radiation transfer equation

The emission and absorption processes in plasmas are described by the radiation transfer equation [1]. The calculation method is the same as that in ref. 7, basically. The radiation transfer equation is solved in a slab model under the following assumptions. The emissivity is calculated using the extended Trubnikov's expression in a tenuous plasma. The electron velocity-distribution function is assumed to be the spherically symmetric relativistic Maxwellian. The absorption coefficient is obtained from the emissivity applying Kirchhoff's law [1]. The plasma has cylindrical symmetry except for B_t. The structure of toroidal magnetic field is taking into account of radial dependence. The ray refractive index for wave propagation is taken as unity in tenuous plasma and the ECE is assumed to propagate in a straight line; *i.e.*, the refraction is neglected. The θ_B is defined the angles between the incoming wave number $\boldsymbol{k}$ and B_t. The θ_{port} is defined the elevation angle between the $\boldsymbol{k}$ and the equatorial plane. Since the refractive indices at the $2.0 \times 10^{20}\,\mathrm{m}^{-3}$ and $8 \times 10^{19}\,\mathrm{m}^{-3}$ are 0.7 in the case of $B_t = 4\,\mathrm{T}$ for 2nd harmonic X mode and fundamental O mode, respectively, the value of $2.0\times10^{20}\,\mathrm{m}^{-3}$ and $8 \times 10^{19}\,\mathrm{m}^{-3}$ are considered to be the limits of a tenuous plasma for 2nd X mode and fundamental O mode, respectively. Reflection at the wall is not considered in the calculation. The propagation is taken account of the non-propagation property due to the upper hybrid resonance. The profiles T_e and n_e are assumed be parabolic function and uniform, respectively. The major and minor radii, R_0, a and B_t are 3.4 m, 1 m, and 4 T for JT-60U, respectively except for Fig. 8.

3. Calculation Results

We calculate the ECE spectra of X and O mode for various θ_B from the LFS observation in the case of $n_e = 5\times10^{19}\,\mathrm{m}^{-3}$, $T_e(0) = 25\,\mathrm{keV}$, $B_t = 4\,\mathrm{T}$. The results of X and O mode are shown in Figs. 1 and 2, respectively. In the case of X mode, $\theta_B \geq 60°$, radiation temperatures seem to be almost close to the T_e in lower frequency side of assumed T_e around 2nd and 3rd harmonics. Actually the $\theta_B \geq 75°$ is suitable for the T_e profile measurements. In the case of $\theta_B \leq 30°$, there is small amount of radiation in high frequency region ($f > 600\,\mathrm{GHz}$). Because θ_B is smaller, the peak of emissivity decreases [4, 5]. When the θ_B decreases, the radiation temperature at the high frequency decreases.

In the case of O mode and $\theta_B = 30°$, the radiation temperature in lower frequency of fundamental mode is close the center T_e, that is the maximum T_e. In the case of O mode, $\theta_B \geq 60°$, radiation temperatures seem to be close to the T_e of assumed T_e around fundamental mode. Actually the $\theta_B \geq 75°$ is suitable for the T_e profile measurements. In the case of $\theta_B \leq 30°$, there is small amount of radiation in high frequency region. When the θ_B increases, the radiation temperature at high frequency ($f > 600\,\mathrm{GHz}$) increases for $\theta_B \leq 45°$, decreases for $\theta_B \geq 60°$. The frequency dependence of radiation temperature can be interpreted from the dependence of emissivity on frequency that is shown in Fig. 1 of Ref. 5. There are side peaks of the fundamental mode for $\theta_B \geq 75°$ around 60 GHz and 150 GHz. The schematic diagram of emissivity profile is shown in Fig. 3. The two horizontal lines in the figure correspond to the frequencies of the side peaks. The emission and absorption around $r/a = 0.2$ result in the side peaks.

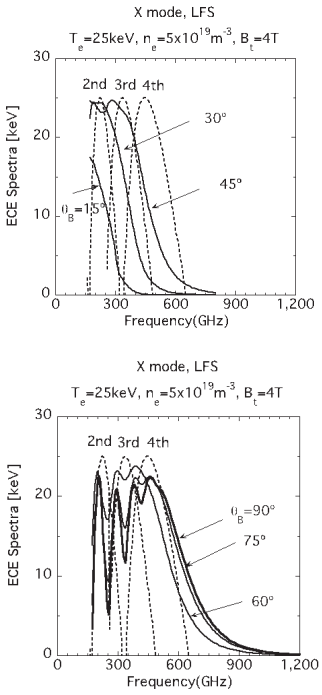

Fig. 1 ECE spectra of X mode for various θ_B in the case of $n_e = 5 \times 10^{19}\,\mathrm{m}^{-3}$, $T_e(0) = 25\,\mathrm{keV}$, $B_t = 4\,\mathrm{T}$, $\theta_{port} = 0°$. The observation is made from low field side. Dotted lines represent radiances that correspond to the assumed $T_e(r)$.

Normally the T_e measurement from ECE is made in the sight line that is perpendicular to B_t and is from LFS in the equatorial plane. The ECE spectra of X and O mode for various n_e from the LFS observation ($\theta_{port} = 0°$) in the case of $\theta_B = 90°$, $T_e(0) = 25\,\mathrm{keV}$, $B_t = 4\,\mathrm{T}$ are shown in Fig. 4. When n_e increases, radiation temperature increases. In the case of X mode, radiation temperatures are close to the T_e in lower frequency side of assumed second harmonic T_e. In the case of O mode, the radiation temperatures are close to the T_e in lower and higher frequency sides of assumed fundamental T_e. So, second harmonic X mode and fundamental O mode has been used for the measurement.

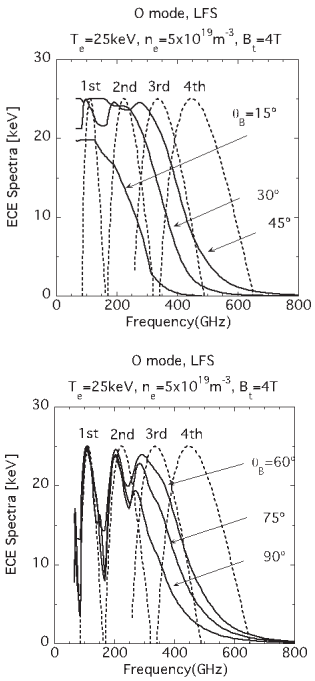

Fig. 2 ECE spectra of O mode for various θ_B in the case of $n_e = 5 \times 10^{19}\,\mathrm{m}^{-3}$, $T_e(0) = 25\,\mathrm{keV}$, $B_t = 4\,\mathrm{T}$, $\theta_{port} = 0°$. The observation is made from low field side. Dotted lines represent radiances that correspond to the assumed $T_e(r)$.

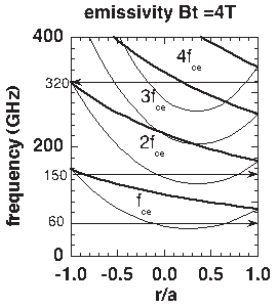

Fig. 3 Schematic diagram of emissivity profile. The relativistic downshift becomes very large at T_e, and the emissivity at the local position has a profile with finite extent in frequency.

We evaluate the ECE spectra that are different from the normal T_e measurement. When the θ_{port} is increased, the overlapping region between second and third harmonics shrinks and the relativistic effect of only one harmonic will be revealed. Specially, in the case of vertical sight line, the radiation is observed from only one resonance frequency region. The ECE spectra of X and O mode for various n_e from the vertical line observation ($\theta_{port} = 90°$) in the case of $\theta_B = 90°$, $T_e(0) = 25\,\mathrm{keV}$, $B_t = 4\,\mathrm{T}$ are shown in Fig. 5. For optically thin case ($n_e = 0.2 \times 10^{19}\,\mathrm{m}^{-3}$), the ECE spectra are similar to the shape of emissivity. The emissivity is given in Fig. 1 of Ref. 5. That is, the 3rd harmonic ECE increases with frequency slowly from the just higher 2nd harmonic non-relativistic EC frequency ($2f_{ce}^0$)

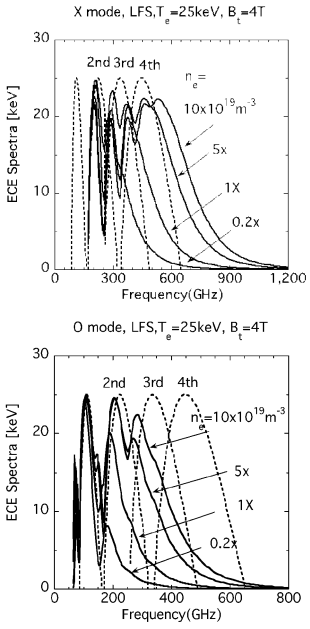

Fig. 4 ECE spectra of X and O modes for various n_e in the case of $T_e(0) = 25\,\mathrm{keV}$, $B_t = 4\,\mathrm{T}$. The observations are made from LFS ($\theta_{port} = 0°$).

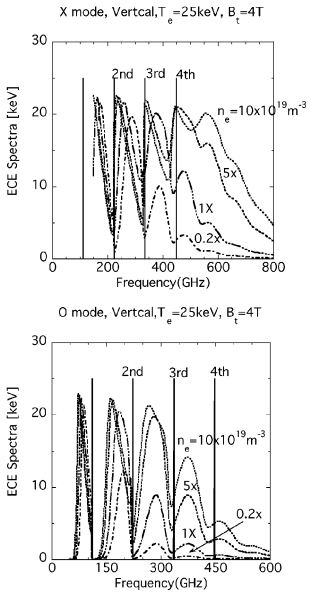

Fig. 5 ECE spectra of X and O modes for various n_e in the case of $T_e(0) = 25\,\mathrm{keV}$, $B_t = 4\,\mathrm{T}$, $\theta_{port} = 90°$.

and decreases with the frequency rapidly to the just lower 3rd harmonic non-relativistic frequency ($3f_{ce}^0$). When the n_e increases, the 3rd harmonic ECE increases with frequency rapidly from the just higher $2f_{ce}^0$, and decreases with the frequency slowly to the just lower $3f_{ce}^0$. The high optical thickness due to the high n_e results in these features.

Next, in the case of the observation from the HFS ($\theta_{port} = 180°$) in the equatorial plane, the ECE spectra of X and O mode for various n_e in the case of $\theta_B = 90°$,

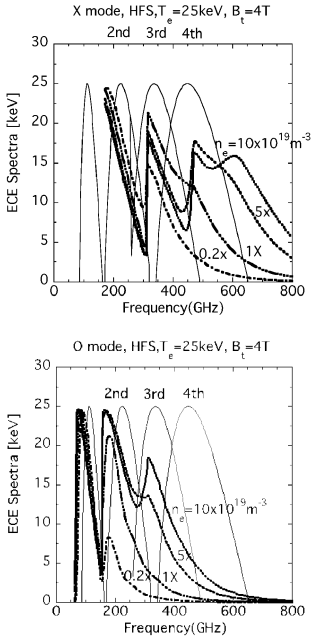

Fig. 6 ECE spectra of X and O modes for various n_e in the case of $T_e(0) = 25\,\mathrm{keV}$, $B_t = 4\,\mathrm{T}$. The observations are made from HFS ($\theta_{port} = 180°$).

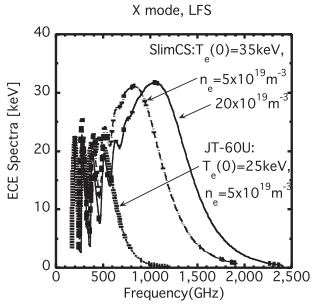

Fig. 7 ECE spectra of X mode for various n_e in the case of SlimCS & JT-60U, $\theta_{port} = 0°$.

$T_e(0) = 25\,\mathrm{keV}$, $B_t = 4\,\mathrm{T}$ are shown in Fig. 6. The down shift frequency due to the relativistic effect in the HFS observation reveals strongly compared with the observation from the LFS. There is the overlapping region of frequency between $(n+1)f_{ce}^0$ at the outer periphery of torus and nf_{ce}^0 at the inner periphery of torus (n = 1-3). The schematic diagram is shown in Fig. 3. The emission is absorbed at the overlapping region, and emission decreases. The combination between the absorption at the HFS plasma of 3rd harmonic and the emission at the LFS plasma of 2nd harmonic results in the deep dip and the peak at 320 GHz.

Japan Atomic Energy Agency (JAEA) has been designing a DEMO reactor SlimCS [12]. The R_0, a and B_t are 5.5 m, 2.1 m, and 6 T, for SlimCS, respectively. ECE spectra of X mode for various $n_e$from the LFS observation ($\theta_{port} = 0°$) in the case of $\theta_B = 90°$ for JT-60U and SlimCS are shown in Fig. 7. In the case of $n_e = 20 \times 10^{19}\,\mathrm{m}^{-3}$, $T_e(0) = 35\,\mathrm{keV}$ of SlimCS, the fusion power is 3 GW. The frequency region is from 100 GHz and 1000 GHz in the case of JT-60U. For comparison of ECE spectra between JT-60U and SlimCS, since the magnetic B_t, n_e and T_e increase, the frequency region expands to the 2500 GHz in the case of SlimCS. When the B_t increases from 3 T to 6 T, the frequency region in the case of 6 T is 1.5 times as wide as that in the case of 4 T. When the n_e increases from $5 \times 10^{19}\,\mathrm{m}^{-3}$ to $20 \times 10^{19}\,\mathrm{m}^{-3}$, the frequency region expands from 2000 GHz to the 2500 GHz in the case of $T_e(0) = 35\,\mathrm{keV}$, SlimCS from Fig. 7. Since the T_e increases from 25 keV to 35 keV, the frequency region also expands. At the present, ECE spectra are measured using Fourier transform spectrometer. The liquid He cooled InSb detector is used, the frequency response is 50 GHz to 1000 GHz. So, ECE detector in the case of Fourier transform spectrometer system should be modified from present liquid He cooled InSb detector because of the detection efficiency.

4. Summary

We evaluated the ECE spectra in the high temperature plasma using the extension of Trubnikov's equation for oblique propagation to B_t in the case of spherically symmetric fully relativistic Maxwellian. Feature of ECE spectra can be interpreted from the viewpoints of relativistic, Doppler and absorption effects. We investigate the ECE for X and O modes by changing the n_e and the angles of θ_B and θ_{port}.

When the θ_B increases, the radiation temperature at high frequency ($f > 600\,\mathrm{GHz}$) increases in the case of X mode and LFS observation ($\theta_{port} = 0°$). In the case of O mode, $\theta_B = 30°$, the radiation temperature in lower frequency of fundamental mode is close the maximum T_e. For the LFS observation, radiations in the fundamental O mode and in the lower frequency side of the second harmonic X mode are close the assumed T_e for $\theta_B \geq 75°$. These modes are used for T_e measurements for $\theta_B = 90°$ normally.

For the vertical observation ($\theta_{port} = 90°$), in the case of optically thin case, ECE spectra are similar to the emissivity profile. When the n_e is higher, ECE spectra are modified due to the absorption in plasma.

The variation of downshift frequency due to the relativistic effect in the HFS observation ($\theta_{port} = 180°$) is bigger than that in the LFS observation ($\theta_{port} = 0°$). There is the overlapping region of frequency between $(n+1)f_{ce}^0$at the outer periphery of torus and nf_{ce}^0 at the inner periphery of torus ($n = 1, 2$). The combination between the absorption at the HFS plasma of $(n+1)$-th harmonic and the emission at the LFS plasma of nth harmonic results in the deep dip and the peak near the overlapping region.

Since the B_t, n_e, T_e become large in the case of the SlimCS DEMO reactor, the ECE spectra expands to high frequency emission ($\sim$ 2000 GHz). So, ECE detector in the case of Fourier transform spectrometer system should be modified from present liquid He cooled InSb detector because of the detection efficiency.

[1] G. Bekefi, *Radiation Processes in Pasmas* (John Wiley and Sons, New York, 1966).
[2] M. Bornatici, R. Cano *et al.*, Nucl. Fusion **23**, 1153 (1983).
[3] A.E. Costley, R.J. Hastie, J.W.M. Paul *et al.*, Phy. Rev. Lett, **33**, 758 (1974).
[4] M. Sato and A. Isayama, *Proc of 14th Joint Workshop on ECE and ECH*, Santorini Greece, 2006, p.205.
[5] M. Sato and A. Isayama, Fusion Sci. Technol. **52**, 169 (2007).
[6] B.A. Trubnikov, *Magnetic Emission of High-Temperature Plasma, Thesis, Institute of Atomic Energy, Moscow, 1958* [English translation: USAEC, tech, Information service, AEC-tr-4073 June 1960].
[7] M. Sato, S. Ishida *et al.*, J. Phys. Soc. Jpn. **62**, 3106 (1993).
[8] H.P. Freund and C.S. Wu, Phys. Fluids **20**, 963 (1977).
[9] I. Fidone and G. Granata, Plasma Physics **21**, 315 (1979).
[10] I. Fidone, G. Granata, R.L. Meyer, E.H. Jornada, R.S. Schneider *et al.*, Phys. Fluids **23**, 1336 (1980).
[11] F. Albajar, N. Bertelli *et al.*, *Proc of 14th Joint Workshop on ECE and ECH*, Santorini Greece, 2006, p.283.
[12] K. Tobita, S. Nishio, M. Enoeda, M. Sato, T. Isono *et al.*, Fusion Eng. Des. **81**, 1277 (2006).